Rats exhibit higher hepatic stress response pathway capacities compared with mice and humans

Giusy Russomanno[1], Rowena Sison-Young[1], Lucia A. Livoti[1], Hannah Coghlan[1], Rosalind E. Jenkins[1], Steven J. Kunnen[2], Ciarán P. Fisher[3], Dennis Reddyhoff[3], Iain Gardner[3], Adeeb H. Rehman[1,4], Stephen W. Fenwick[4], Andrew R. Jones[5], Guy Vermeil De Conchard[6], Gilles Simonin[6], Helene Bertheux[6], Richard Weaver[6], Michael J. Liguori[7], Diana Clausznitzer[8], James L. Stevens[2], Christopher E. Goldring[1], Ian M. Copple[1]*.

[1]MRC Centre for Drug Safety Science, Department of Pharmacology & Therapeutics, Institute of Systems, Molecular & Integrative Biology, University of Liverpool, Liverpool, UK.

[2]Division of Drug Discovery and Safety, Leiden Academic Centre for Drug Research (LACDR), Leiden University, Leiden, The Netherlands.

[3]Simcyp Division, Certara UK, Sheffield, UK.

[4]Department of Hepatobiliary Surgery, Aintree University Hospital, Liverpool University Hospitals NHS Foundation Trust, Liverpool, UK.

[5]Department of Biochemistry & Systems Biology, Institute of Systems, Molecular & Integrative Biology, University of Liverpool, Liverpool, UK.

[6]Translational Medicine, DMPK, Bioanalysis, Technologie Servier, 45007 Orléans Cedex, France.

[7]Pre-Clinical Safety, AbbVie Inc., Chicago, Illinois, USA.

[8]DMPK-BA, AbbVie Deutschland GmbH & Co. KG, Ludwigshafen, Germany.

*Corresponding author: ian.copple@liverpool.ac.uk

Acknowledgements

This work is dedicated to the memory of B. Kevin Park, the founding coordinator of the TransQST consortium, who died during the preparation of this manuscript. We acknowledge the contributions of Technologie Servier staff to the in-life phases of this work (Sylvie Roussel, Anne Marchau, Christine Bubois, Nathalie Delory), the clinical pathology (Claudette Chevalier, Laura Bochet), the histopathology (Eric Jacquemin, Catherine Cador, Laurent Gindrey, Jean-Pierre Creusillet, Agathe Buvat), the bioanalysis (Nathalie Landerouin, Jacky Pothier), and the tissue preparation (Laurence Launay, Laurence Proust). We also acknowledge the contributions of AbbVie staff to the RNA extraction (Clarissa Woody) and the microarray analysis (Rita Ciurlionis).

Funding

We acknowledge financial support from the TransQST consortium, which received funding from the Innovative Medicines Initiative 2 Joint Undertaking under grant agreement no. 116030. This Joint Undertaking receives support from the European Union's Horizon 2020 research and innovation program and EFPIA. This work was also supported by the Medical Research Council (MRC) as part of the Centre for Drug Safety Science (MR/L006758/1).

Abbreviations

ACN, acetonitrile; ALT, alanine aminotransferase; APAP, acetaminophen; AST, aspartate aminotransferase; AUC, area under the curve; BCA, bicinchoninic acid; CHAPS, 3-[(3-cholamidopropyl)dimethylammonio]-1-propanesulfonate; DDA, data-dependent acquisition; DEGs, differentially expressed genes; DIA, data-independent acquisition; DILI, drug-induced liver injury; EDTA, ethylenediaminetetraacetic acid; ER, endoplasmic reticulum; FDR, false discovery rate; GAPDH, glyceraldehyde 3-phosphate dehydrogenase; GCLC, glutamate-cysteine ligase catalytic subunit; GCLM, glutamate-cysteine ligase modifier subunit; GFR, glomerular filtration rate; GO, gene ontology; GSEA, gene set enrichment analysis; GSH, glutathione; HES, haematoxylin-eosin saffron; HMOX1, heme oxygenase 1; HPLC, high-performance liquid chromatography; IPA, Ingenuity Pathway Analysis software; JNK, c-Jun N-terminal kinase; Keap1, Kelch-like ECH-associated protein 1; LC3B, microtubule-associated proteins 1A/1B light chain 3B; LD50, lethal dose 50; LW, liver weight; MW,

molecular weight; NAC, N-acetyl cysteine; NAPQI, N-acetyl-p-benzoquinoneimine; NES, normalised enrichment score; NQO1, NAD(P)H quinone dehydrogenase 1; Nrf2, nuclear factor-erythroid factor 2-related factor 2; OED, oral equivalent dose; PBPK, physiologically-based pharmacokinetic; p-JNK, phosphorylated c-Jun N-terminal kinase; RPKM, reads per kilobase per million; SDS, sodium dodecyl sulfate; SQSTM1, sequestosome 1; SWATH, sequential window acquisition of all theoretical mass spectra; TBIL, total bilirubin; WGCNA, weighted gene co-expression network analysis.

ABSTRACT

In order to minimise the occurrence of unexpected toxicities as a new medicine transitions from the preclinical to clinical phases of development, it is vital to understand fundamental similarities and differences between preclinical species and humans. The well-known difference in sensitivity of mice and rats to acetaminophen (APAP) liver injury has been related to differences in the fraction that is bioactivated to the reactive metabolite N-acetyl-p-benzoquinoneimine (NAPQI). We have used physiologically-based pharmacokinetic modelling to identify doses of APAP (300 and 1000 mg/kg in mice and rats, respectively) yielding similar hepatic burdens of NAPQI to enable the comparison of temporal liver tissue responses under conditions of equivalent chemical insult. Despite pharmacokinetic and biochemical verification of the equivalent NAPQI insult, serum biomarker and tissue histopathology analyses revealed that mice still exhibited a greater degree of liver injury than rats. Transcriptomic and proteomic analyses highlighted the stronger activation of stress response pathways (including the Nrf2 oxidative stress response and autophagy) in the livers of rats, indicative of a more robust transcriptional adaptation to the equivalent insult. Using RNA-Seq data, we also found that genes associated with these stress responses are expressed at a higher basal level in the livers of rats compared with both mice and humans. Taken together, these data indicate that rats possess a greater basal and adaptive capacity for hepatic stress responses than mice and humans. This has important implications for species selection in preclinical safety testing of drugs associated with reactive metabolite formation and other forms of chemical stress.

INTRODUCTION

A critical stage in the development of a new medicine is the transition from preclinical experiments to trials in humans. The success of this transition is dependent on the robust translation of preclinical findings to clinical responses, in terms of both efficacy and safety (1, 2). For example, there are numerous cases where a drug candidate has caused serious liver toxicity in patients despite preclinical safety assessment indicating no cause for concern (3-5). On the other hand, many developmental compounds deemed unsafe in preclinical species may have been found to be safe in humans. In order to minimise the occurrence of unexpected clinical toxicities and improve the efficiency of the drug development process, it is vital to understand fundamental similarities and differences amongst and between preclinical species and humans, to inform the selection of appropriate preclinical models, and so accurately predict clinical responses based on in vivo and in vitro data. Conceptually, differential adverse effects of a drug in different species may be a result of dissimilar toxicokinetics and/or toxicodynamics. More specifically, the differential response to a drug may be driven by (a) differences in its disposition (e.g. a toxic metabolite is formed to a greater extent in the sensitive species, such as with the hepatotoxin acetaminophen (APAP) (6)), (b) the differential expression of a target protein (e.g. the equilibrative nucleoside transporter 1, in the case of fialuridine liver toxicity (7)) or (c) fundamental differences in the nature and/or extent of the downstream cellular response to chemical insult. Whilst (a) and (b) have been extensively studied in the context of various drug toxicities, (c) has garnered less attention to date.

APAP is the single largest cause of acute liver failure in the UK and US (8, 9), and is commonly used as an exemplar drug for studying hepatotoxicity. APAP is metabolically bioactivated to the highly reactive N-acetyl-p-benzoquinonimine (NAPQI) which depletes glutathione (GSH) stores, induces oxidative stress and covalently reacts with hepatocellular proteins leading to necrosis (10, 11). It is well known that mice (oral LD50 ~350 mg/kg) are relatively sensitive to APAP liver injury compared with rats (oral LD50 ~2000 mg/kg) (6). Previous work has indicated that this disparity is related to species differences in the fraction of APAP that is bioactivated to NAPQI, with mice exhibiting a higher fraction of APAP metabolised to NAPQI (12-14). To account for this species difference, and better design a comparative study of the response of mice and rats to APAP insult, we have used physiologically-based pharmacokinetic (PBPK) modelling and simulation to identify doses of APAP yielding an equivalent hepatic burden of NAPQI in the two species. Using this approach, we compare changes in the transcriptome and proteome of mice and rats following exposure to equivalent APAP insult, and reveal marked differences between the rodent species, and humans, in the basal and adaptive capacities of hepatic stress response pathways that are known to influence APAP toxicity and other forms of drug-induced liver injury (DILI). Our findings have important implications for the selection of preclinical models during the toxicity assessment of new drug candidates.

METHODS

PBPK modelling

Physiologically-based pharmacokinetic (PBPK) models were constructed using the Simcyp Animal simulator (v18r2; Certara Inc., Simcyp Division, Sheffield, UK) to predict the disposition of APAP and its metabolites arising from sulphation, glucuronidation, and cytochrome P450 mediated metabolism and glutathione conjugation of the resultant reactive-metabolite, NAPQI. Details of the animal PBPK simulators and the QA system used in the development of each version of the Simcyp simulator have been described previously (15-18). Models were parameterised and their predictive performance verified using data from the peer-reviewed literature. Verified PBPK models in each species were used to perform simulations to determine oral equivalent doses (OED; mg/kg body weight). Here the OED is defined as the orally-administered APAP dose resulting in a total hepatic NAPQI burden equivalent between the species of interest. Predicted OEDs were used as doses in the in vivo time course study described below. Data from this study was then analysed to determine the total hepatic NAPQI burden in each species. Two independent analyses of study data were performed based on mass balance analysis of all metabolites or total hepatic GSH depletion; due to the availability of data, the former approach could only be applied in the mouse. For the mass balance approach, the glutathione (1), cysteine (2) and N-acetyl cysteine (3) conjugated APAP metabolites were considered as the three relevant metabolites derived from NAPQI. An area under the plasma concentration time curve (AUC; mg/L.h) for NAPQI metabolite was calculated based on the sum of the individual metabolite AUCs corrected for the molecular weight (MW) of NAPQI (149.2 g/mol). This was then scaled to a total hepatic NAPQI burden (mg/g

liver) assuming passive renal filtration (GFR_{mouse} = 0.0144 L/h) and 30 % biliary clearance (equation x)

$$Total\ Hepatic\ Burden_{NAPQI} = \frac{\sum_{i=1}^{n=3} AUC_i}{MW_{NAPQI} \cdot 10^{-3}} \cdot GFR \cdot \frac{1}{(0.7 \cdot LW)}$$

Equation x

Based on glutathione depletion, total hepatic NAPQI burden was calculated by determining the loss of GSH based on the average GSH level (nmol) in control animals and the minimum GSH level in APAP dosed animals; this was then converted to a total hepatic burden (mg/g liver) assuming a 1:1 stoichiometry between NAPQI and glutathione (equation y).

$$Total\ Hepatic\ Burden = \frac{\mu_{GSH,control} - min_{GSH,APAP}}{MW_{NAPQI} \cdot 10^{-6}} \cdot \frac{1}{LW}$$

Equation y

Liver weight (LW) was taken as 1.3 g and 9.0 g for mouse and rat, respectively; protein content was assumed to be 250 mg/g liver for both species.

Animals and dosing

Animal experiments were performed at Biologie Servier (France) in accordance with the European Council Directive 2010/63/EU on the protection of animals used for scientific purposes. The studies were approved by both Biologie Servier and TransQST consortium ethical review committees. For the dose-ranging study, male

C57Bl/6J mice (8 weeks old; 15-22 g body weight; n=5 per dose) or Sprague-Dawley rats (5 weeks old; 119-144 g body weight; n=5 per dose) were fasted for 16 h prior to dosing. APAP (Sigma-Aldrich) was solubilised in 1 % (w/v) hydroxyethylcellulose (Sigma-Aldrich). Mice were administered 150, 300, 450 or 600 mg/kg APAP by oral gavage. Rats were administered 1000, 1300 or 1600 mg/kg APAP by the same route. Vehicle control groups were administered 1 % hydroxyethylcellulose. For the time course study, fasted mice (n=5 per time point) and rats (n=5 per time point) were administered 300 mg/kg and 1000 mg/kg APAP, respectively, or vehicle, by oral gavage. At relevant time points, the animals were sacrificed by exsanguination under isoflurane anaesthesia. Liver tissue and blood samples were collected at baseline (0 h) and at 3, 6, 9 and 24 h after administration of APAP or vehicle for the analyses described below.

Serum biomarker analysis

Blood samples were collected from a jugular vein or abdominal aorta of isoflurane-anaesthetised animals into tubes with a serum separator. Blood samples were centrifuged at top speed after clotting and analysed using a Cobas c501 analyzer (Roche). Alanine aminotransferase (ALT) and aspartate aminotransferase (AST) activities were measured kinetically at 37 °C according to the International Federation of Clinical Chemistry recommendations without Pyridoxal Phosphate (Roche). Total bilirubin (TBIL) was measured using 3,5-dichlorophenyl diazonium (Roche).

Liver glutathione content measurement

Liver tissue was homogenised in buffer (pH 7.4) comprising 143 mM NaH_2PO_4, 8 mM EDTA and 1.3 % sulfosalycilic acid, using an oscillating mill at 30 oscillations/sec for

3 min. The homogenates were then centrifuged (18,000 g for 5 min at 4 °C) and the supernatants collected. Total glutathione (GSH) was measured as described previously (19). The reaction was followed kinetically at 415 nm. Sample readings were interpreted against a GSH calibration curve and normalised to protein content, which was determined from the sample pellets (dissolved in 1 M NaOH at 60 °C) generated during the homogenisation step, using the bicinchoninic acid method (Sigma-Aldrich).

Pharmacokinetic analysis

Plasma samples (collected in heparin-coated tubes and stored at -80 °C until analysis) were thawed at room temperature and centrifuged (3000 g for 5 min at 4 °C). Each sample (10 µL) was then spiked with 10 µL internal standard (8 µg/mL for APAP d4 and APAP Gluc d3, 9 µg/mL for APAP Sul d3 and 0.6 µg/mL for APAP NAC d5, APAP Cys d5 and APAP GSH d3; all in MeOH) or MeOH alone as blank. Proteins were precipitated from each sample by adding 180 µL MeOH, mixed (1500 rpm for 5 min), stored at -20 °C for 20 min, centrifuged (3000 g for 5 min at 4 °C) and the supernatants collected. Each sample was further diluted with 600 µL water, mixed (800 rpm for 2 min), centrifuged (3000 g for 5 min at 4 °C) and the supernatant used for injection into the UPLC-MS/MS system.

The samples were analysed using an UPLC-I Class system (Waters) coupled to an API 4000 QTrap mass spectrometer (Sciex). Separation was performed using an Acquity UPLC HSS T3, 1.8 µm, 100 x 2.1 mm with a 0.2 µm pre-filter (Phenomenex) and a column oven set to 40 °C. The injection volume was 2 µL and flow rate 0.6 mL/min. The mobile phases and gradient programme are summarised in

Supplementary Table S1. Mass spectrometric analysis was performed in either positive or negative ion mode, as detailed in Supplementary Tables S2 and S3.

Histopathological assessment

For each animal, the entire liver (gall bladder was carefully removed for the mouse) was rapidly excised and briefly rinsed in DNase/RNase -free distilled water. The left liver lobe was then separated and preserved in 10 % formalin. Fixed samples were mounted in paraffin wax, cut at approximately 4 µm in thickness, stained with haematoxylin-eosin saffron (HES) and evaluated by two independent veterinary pathologists. The extent of centrilobular hepatocellular necrosis/degeneration was assigned a consensus semi-quantitative score as follows: 0, no degeneration/necrosis observed; 1, minimal degeneration/necrosis of individual or small groups of hepatocytes; 2, mild degeneration/necrosis that bridges some centrilobular zones; 3, moderate degeneration/necrosis that completely bridges centrilobular zones; 4, marked degeneration/necrosis that bridges centrilobular zones and extends into midzone areas; 5, severe degeneration/necrosis involving all hepatic lobular zones.

Immunoblotting

Snap frozen liver tissue (30-40 mg) was homogenised in radioimmunoprecipitation buffer (Sigma Aldrich). Liver homogenate (20 µg) was separated by SDS-PAGE under reducing conditions, transferred to nitrocellulose membranes and subjected to immunoblot analysis as previously described (20). Details of all antibodies used in this study are provided in Supplementary Table S4. Immunoreactive bands were visualised using a ChemiDoc Imaging System (Bio-Rad) and volumes were quantified using Image Lab Version 6.1.0 (Bio-Rad), with normalisation to β-actin. For the

representative blots, a pool of all samples for each treatment group and time point were loaded onto the gel.

Transcriptomic analysis

Total RNA was isolated from liver tissue collected in RNAlater® stabilizing reagent immediately prior to dosing (0 h) or at 3, 6, 9, and 24 h after administration of APAP or vehicle. Frozen liver samples were homogenised in Qiazol Lysis Reagent (Qiagen). Total RNA was purified following the manufacturer's instructions from Qiagen. The RNA integrity in representative samples was verified using an Agilent BioAnalyzer. Total RNA (5 µg) was processed per the standard Affymetrix protocol for microarray target preparation. Resulting cRNA was fragmented and hybridized onto Affymetrix GeneChips, which were then washed, stained, and scanned using the standard Affymetrix procedure (Affymetrix GeneChip® Mouse Genome 430 2.0 Array or Affymetrix GeneChip® Rat Genome 230 2.0 Array). Quality control and low level analysis of raw fluorescence intensities was performed using the affy package (v1.64.0) in R v3.6.1 (21). Mouse data were processed using RMA normalization and BrainArray CDF Version 24 (22). Rat data were processed using RMA normalization and BrainArray CDF Version 19, which gives 100 % coverage on the DILI TXG-MAPr tool (https://txg-mapr.eu/) used for Weighted Gene Co-Expression Network Analysis (WGCNA). Differential expression analyses were carried out using the limma package (v3.42.2) in R (23). Using the Rat Genome Database (RGD) orthologous genes between rat and mouse were considered for comparison of the transcriptomic changes. Genes were considered differentially expressed when the adjusted P value (Benjamini-Hochberg correction) was less than 0.05 and there was at least a 1.5-fold change in expression. The full list of significant genes at each time point was analysed

for membership in co-expressed gene sets using WGCNA, as previously described (24).

Pathway analysis

ClusterProfiler package (v3.18.0) (25) was used for gene set enrichment analysis (GSEA) on the lists of differentially expressed genes (DEGs) ranked by $\log_2$ fold-change. The number of permutations was set to 10,000. To remove differences in the setSize, genome wide annotation for Rat (package 'org.Rn.eg.db') was used for both species. Gene ontology (GO) biological processes (26) were considered significantly enriched with a FDR-corrected $P_{adj} < 0.05$ and absolute Normalised Enrichment Score (NES) >1.5. Genes that were differentially expressed in either species at any time point within the lists of enriched genes in selected GO biological processes were used to generate heatmap plots showing changes at a gene level between species (data expressed as $\log_2$ fold-changes *versus* time-matched vehicle controls animals).

qPCR analysis

RNA (500 ng) was reverse transcribed using a LunaScript RT SuperMix kit (New England Biolabs) according to the manufacturer's instructions in a total 20 µL reaction mix. qPCR was performed using Luna Universal qPCR Master Mix (New England Biolabs) on an ABI ViiA-7 Thermocycler (Applied Biosystems). Primer sequences for mouse and rat genes are detailed in Supplementary Table S5. For relative quantification, data were analysed using the $2^{-\Delta\Delta Ct}$ method. The selection of GAPDH as the endogenous normalization control was based on analysis of the transcriptomic data using NormFinder (27), which ranked homologous genes with a coefficient of

variation < 1% across treatments and time points, based on the calculated stability values.

Proteomics sample preparation

Liver tissue (100-200 mg) was lysed by sonication on ice in 300 µL of 7 M urea, 2 M thiourea, 40 mM tris (pH 7.5) and 4 % w/v CHAPS buffer. After centrifugation (14,000 rpm for 10 min at 4 °C), the supernatant was collected and protein concentration was determined by Bradford assay. Next, 200 µg protein was reduced with 5 mM dithiothreitol at 37 °C for 30 min, alkylated with 0.15 M iodoacetamide, and incubated at 37 °C for 3 h with Trypsin/Lys-C (Promega) at a 25:1 protein:protease ratio (w/w). The reaction mix was then diluted 1:10 with 50 mM ammonium bicarbonate in order to reduce the urea concentration to less than 1 M, and incubated overnight at 37 °C. Peptides were then diluted to 5 mL with 10 mM potassium dihydrogen phosphate/25 % acetonitrile (ACN) and acidified to pH ≤ 3 with phosphoric acid prior to cation exchange chromatography. In order to generate the reference spectral libraries, a pool of 20 samples/species representative of all the experimental conditions was prepared. An aliquot of 1.5 mg of the pool was pre-fractionated on a Polysulfoethyl A column (200 × 4.6 mm, 5 µm, 300 A; Poly LC) at a flow rate of 1 mL/min. For individual samples, detergents and undigested protein were removed using a Bio-Scale Mini Macro-Prep High S 1 mL cartridge (Bio-Rad) on an Agilent 1100 HPLC system at 1 mL/min. The mobile phases consisted of 10 mM KH_2PO_4/25 % ACN w/v, pH 3 (phase A), and 10 mM KH_2PO_4/1 M KCl/25 % ACN w/v, pH 3 (phase B). A gradient from 0-50 % B in 90 min was applied to the Polysulfoethyl A column. Peptides were eluted from the cartridge using a gradient time program set as follows (phase B): 0 %; 0-0.5 min, 0-15 %; 0.5-5 min, 15 %; 5-5.10 min, 15-50 %; 5.10-7 min, 50 %; 7-7.10

min, 50-0 %; 7.10-10 min, 0 %. The system was then washed with 100 % phase A for 5 min after each sample to prevent sample carryover. Fractions of 1 mL were dried in a SpeedVac Concentrator Plus (Eppendorf), then reconstituted in 1 mL of 0.1 % trifluoroacetic acid and desalted using an Agilent Macroporous Reversed-Phase C18 column (4.6 × 50 mm mRP-C18, Agilent) on an Agilent 1260 Infinity HPLC system (Agilent).

Data-dependent acquisition (DDA) and data analysis

Desalted fractions were reconstituted in 0.1 % formic acid and 0.5-1 µg of sample was loaded onto a UPLC Symmetry C18 nanoAcquity Trap Column (Waters). After a 10 min wash with 2 % ACN/0.1 % formic acid, the trap was switched in-line with a peptide BEH C18 nanoAcquity column (1.7 µm, 75 µm x 250 mm; Waters) and a gradient of 2-50 % ACN/0.1 % formic acid was applied over 120 min at a flow rate of 300 nL/min. DDA was performed on a Triple TOF 6600 (Sciex) in positive ion mode with a target of 25 MS/MS per cycle (2.8 sec cycle time), exclusion of former target ions for 20 sec, and using a mass range of 400-1800 for MS and 100-1500 for MS/MS. The data were searched using ProteinPilot 5.0 (Sciex) and the Paragon algorithm (Sciex) against the UniProtKB database (Mus musculus UP000000589, gene count 22,001, 55,366 proteins, last modified March 2021; Rattus norvegicus UP000002494, gene count 21,588, 29,934 proteins, last modified March 2021). Proteotypic peptides with no modifications except carbamidomethylation of cysteine residues were included in the library, so a ‘rapid’ search of the data was performed using ProteinPilot. Mass tolerance for precursor and fragment ions was 10 ppm. A FDR of 1 % was applied using the reversed database as decoy. This resulted in 5,253 and 5,823 proteins being included in the mouse and rat libraries, respectively.

SWATH acquisition and data analysis

The same sample loading and chromatography conditions as described above were used for the individual sample acquisitions. Sequential Window Acquisition of all Theoretical Mass Spectra (SWATH) acquisitions were performed using 100 SWATH windows of variable effective isolation width to cover a mass range of 400-1600 m/z. The total cycle time was 3.1 sec. To account for batch effects, a pool of 20 samples representative of all the experimental conditions and a yeast digest quality control (Promega) were included with the samples in each batch. SWATH data were aligned with the spectral libraries using DIA-NN (v1.8) (28) with default settings in 'robust LC (high accuracy)' mode and annotated using the reference proteomes (UP000000589 and UP000002494) downloaded as FASTA files. Mass tolerances were determined automatically in DIA-NN for each run separately (Unrelated runs option). Match-between-runs was enabled to re-process the same dataset using a spectral library generated from the data-independent acquisition (DIA) data. Only proteins identified with proteotypic peptides and protein q-value below 0.01 were considered. Normalisation and differential expression analyses were carried out using the DEqMS package (v1.8.0) (29) in R. Protein quantities were $\log_2$ transformed and normalised using the equalMedianNormalization function, and Limma batch effect correction was applied. Ingenuity Pathway Analysis software (IPA; Qiagen) was used to investigate enriched canonical pathways and toxicity functions (IPA-Tox) in the two species. Comparison analyses were performed to evaluate changes in the z-score for each function over time and across species and reveal biological pathways underlying toxicity-specific phenotypes. Since the mouse and rat SWATH datasets were analysed separately, $\log_2$ transformed normalised protein expression values of orthologous proteins from the 0 h control animals (untreated) were ranked and grouped into 10

bins within each dataset for comparison of basal protein abundances across species (30). Proteins with the lowest protein abundance values were assigned to bin 1, whereas those with the highest abundance values were assigned to bin 10. Proteins that were not detected (NA, not available) were assigned a bin value of 0.

Analysis of public RNA-Seq data

To assess basal expression levels of relevant genes in liver tissue from humans, mice and rats, publicly available RNA-Seq data from Cadoso-Moreira *et al.* (31) were used (https://apps.kaessmannlab.org/evodevoapp/). Hepatic mRNA levels (reads per kilobase per million, RPKM) in humans (ArrayExpress E-MTAB-6814), mice (E-MTAB-6798), and rats (E-MTAB-6811) were compared. Human samples were grouped as follows: “neonates”, “infants” (6-9 months), “toddlers” (2-4 years), “school” (7-9 years), “teenagers” (13-19 years), “adults” (25-32 years), “middle-aged” (45-54 years), and “seniors” (58-63 years). Mouse samples (strain CD1, RjOrl:SWISS) were collected at week 0, 3, 14, 28, and 63, whereas rat samples (strain Holtzman Sprague-Dawley) were collected at week 0, 3, 7, 14, 42, and 112.

Human liver tissue

Human liver tissue was obtained by qualified medical staff at Aintree University Hospital (Liverpool, UK). All patients donated tissue as part of planned liver resections (see Supplementary Table S6 for details). Written, informed consent was obtained from each patient. The study protocol was approved by the National Health Service North West–Liverpool Central Research Ethics Committee (11/NW/0327) and conformed to the ethical guidelines of the 1975 Declaration of Helsinki.

Statistical analysis

Statistical analysis was performed using StatsDirect 3 Software. Normal distribution was assessed by the Shapiro-Wilk test. A two-tailed student's unpaired t-test or one-way ANOVA was used if normality was indicated. For non-normally distributed data, a two-tailed Mann Whitney U or Kruskal Wallis test was applied. Results were considered significant if $P \leq 0.05$.

RESULTS

Identification of pharmacokinetically-equivalent doses of APAP in mice and rats

To date, very little has been done to rigorously compare the response to a given chemical entity across preclinical species in order to identify the species that can better translate to humans. Towards our goal of comparing the liver tissue responses of mice and rats at equivalent doses of the exemplar hepatotoxin APAP, we first performed a dose-ranging study in which male C57Bl/6J mice and Sprague-Dawley rats were administered 150-600 mg/kg or 1000-1600 mg/kg APAP, respectively, by oral gavage. We were unable to test higher doses in rat due to the limited solubility of the drug. Liver injury was assessed by quantification of serum biomarkers and semi-quantitative histopathological evaluation of liver tissue, which were collected 24 h after dosing. Mice exhibited significantly increased activities of serum ALT, AST and TBIL, along with centrilobular hepatocellular degeneration/necrosis, from 300 mg/kg APAP (Supplementary Fig. S1). Whilst these markers were also elevated in rats, the incidence and severity of liver injury was lower than observed in mice (Supplementary Fig. S1), despite the use of much higher doses in the former. Hence, on the basis of serum biochemistry and liver histopathology, it was apparent that equivalent APAP injury could not be achieved in the two species. We therefore used PBPK modelling and simulation to predict oral doses of APAP resulting in an equivalent hepatic NAPQI burden in mice and rats. Using this approach, it was predicted that 300 mg/kg APAP in mice and 1000 mg/kg APAP in rats would result in a similar hepatic NAPQI burden (Fig. 1). We therefore used these doses of APAP to investigate the temporal liver tissue responses of the two species under conditions of equivalent NAPQI insult.

In mice, 300 mg/kg APAP resulted in significant elevations of serum ALT, AST and TBIL activities that peaked 3 h after dosing (Fig. 2A-C). The response to oral administration of APAP was more rapid than previous reports (32, 33), and likely related to enhanced absorption associated with the 1 % hydroxyethylcellulose vehicle. Whilst significant elevations of serum ALT, AST and TBIL activities were also observed in rats dosed with 1000 mg/kg APAP, the peak of the response was detected 9 h after dosing (i.e. later than in mice), and the magnitude of change relative to vehicle treated controls was muted when compared with mice (Fig. 2A-C). Microscopic findings correlated with these serum biomarker changes. In mice, acute degeneration of centrilobular hepatocytes was observed as early as 2 h post-dose (Fig. 2D-E). Degeneration progressed to hepatocellular necrosis over time with peak severity observed at 9 h post-dose. In rats, centrilobular hepatocyte necrosis was only observed at 9 to 24 h post-dose and occurred at lower incidence and severity relative to this finding in mice (Fig. 2D-E). As demonstrated by serum ALT and AST activities returning toward baseline, APAP liver injury was resolving by 24 h in rats, but remained relatively higher at the same time point in mice (Fig. 2A-E, and Supplementary Fig. S2). Taken together, these findings demonstrate that hepatocellular injury occurs more quickly and to a greater magnitude in mice relative to rats when challenged with an equivalent hepatic NAPQI burden.

NAPQI is inherently unstable and difficult to quantify bioanalytically. Therefore, as NAPQI is known to deplete hepatic GSH as a prerequisite for liver injury (10, 11), we first quantified levels of hepatic GSH in order to confirm the equivalence of chemical

insult at the doses of APAP used in mice and rats. In both species, there was a time-dependent increase in GSH in vehicle-treated animals (Fig. 3A), reflecting the restoration of normal resting levels following the reintroduction of food after the 16 h period of fasting prior to APAP dosing. Consistent with the metabolic bioactivation of APAP to NAPQI, there was a significant and equivalent early reduction in GSH in mice and rats treated with APAP (Fig. 3A). In mice, this early depletion was followed by a time-dependent increase in GSH, which reached 55 % of the level quantified in the livers of vehicle-treated controls at 24 h (Fig. 3A). In rats, however, GSH was restored to 86 % of the level of vehicle controls by this point (Fig. 3A), indicating an enhanced capacity of the rat to adapt to the equivalent chemical insult. To verify the similar exposures of the two species to the products of APAP bioactivation, pharmacokinetic analysis was performed on plasma collected from the animals. Quantification of the GSH, N-acetylcysteine and cysteine conjugates of APAP revealed similar levels in the two species (Fig. 3B-D). Total hepatic NAPQI burden was calculated to assess whether PBPK modelling and simulation had predicted OEDs between the two species. Based on GSH depletion, total hepatic NAPQI burdens of 1.36 mg/g liver and 0.97 mg/g liver were calculated for mouse and rat, respectively. Based on mass balance, a total hepatic NAPQI burden of 0.63 mg/g liver was calculated for mouse; it was not possible to apply this approach in rat due to the absence of data at early time points. These calculations from the study data indicate that the PBPK predicted OEDs for mouse and rat, 300 mg/kg and 1000 mg/kg, respectively, achieved total hepatic burdens within 1.4 to 1.6 -fold between the two species. Absolute PBPK predictions of total hepatic burden were within 2 to 3 -fold of values derived from experimental data for both species.

In keeping with the larger dose of APAP administered to rats, both the glucuronide and sulphate conjugates were detected at higher concentrations in time-matched plasma samples compared with mice (Fig. 3E-F). In a further demonstration of the comparable extent of chemical insult in the two species, we detected phosphorylation of c-Jun N-terminal kinase (p-JNK) in mice and rats peaking 3 h after APAP administration (Fig. 3G-H). Phosphorylation and subsequent mitochondrial translocation of JNK is reported to be a critical step in the mechanism of APAP hepatotoxicity (6). Whilst the normalised levels of p54- and p46- JNK appeared relatively higher in mice, this was largely influenced by the higher basal level of total JNK in rats (Fig. 3G-H), as reported by others (6). Together, these data confirm the equivalence of chemical insult in the livers of mice and rats treated with 300 and 1000 mg/kg of APAP, respectively.

Rats exhibit a more robust activation of adaptive stress response pathways than mice in response to an equivalent APAP insult

To explore the tissue responses of mice and rats to an equivalent APAP insult, we performed transcriptomic analysis on liver tissue collected from each species following administration of vehicle or the APAP OEDs. The expression of several hundred genes was commonly altered in both mice and rats over the 24 h study period (Fig. 4A), indicating a degree of similarity in the transcriptional response to APAP across the species. However, whilst approximately 300 genes were uniquely responsive to APAP insult at each time point in the mouse, a far greater number of genes (peaking at 1819 genes by 9 h post-APAP administration) were found to be differentially expressed only in the rat (Fig. 4A), suggesting a more robust overall transcriptional response to the equivalent APAP insult in the latter species.

Consistent with the relative degrees of drug-induced tissue injury observed in the two species, mice were found to exhibit a stronger early activation of processes involved in regulation of cell death, apoptosis and inflammatory and immune responses, compared with rats (Fig. 4B-C). Moreover, the activation of these processes and associated genes had diminished by 24 h after APAP administration in rats but not in mice (Fig. 5A-B), suggestive of a more robust adaptation in the former species. On the other hand, rats exhibited a stronger activation of the Nrf2-driven response to chemical and oxidative stress, along with markers of the endoplasmic reticulum stress response and autophagy, which is a catabolic process that enables the recycling of cellular components and damaged organelles under conditions of stress (34) (Fig. 4B-C and 5C-E). These findings were further confirmed by weighted gene co-expression network analysis (WGCNA; Supplementary Fig. S4). The altered expression of representative genes from these processes was confirmed at each time point in the two species via qPCR (Supplementary Fig. S5), which showed an excellent correlation with the corresponding transcriptomics data (Supplementary Fig. S6). Given that the APAP study was conducted in animals fed with a diet known to contain relatively high levels of arsenic (35), a heavy metal known to influence Nrf2 activity (36, 37), we compared the basal expression of Nrf2-regulated genes in the livers of mice and rats fed with diets containing high (A04) and low (RM1) levels of arsenic. There was a trend towards lower expression of these genes in the livers of animals fed the high arsenic diet (Supplementary Fig. S7), indicating that the more robust activation of Nrf2 and other adaptive stress responses in rats following the equivalent NAPQI insult is not associated with the diet used in the study.

To confirm that the apparent species differences in response to the equivalent APAP insult were preserved at the protein level, quantitative SWATH proteomics analysis was carried out on liver tissues collected from the vehicle and APAP-treated animals. Given the time required for transcriptional responses to manifest in altered protein expression levels, we focused on the samples collected 6, 9 and 24 h after dosing, and performed Ingenuity Pathway Analysis (IPA) to understand the pathway level effects of the observed protein expression changes. Liver tissue from APAP-treated mice showed activation of toxicity functions associated with liver injury and cell apoptosis, whereas liver tissue from rats exhibited stimulation of hepatocyte proliferation processes, further evidencing the different extents of adaptation between the two species (Fig. 6A). Consistent with the observed gene level changes, liver tissue from APAP-treated rats showed a greater increase in the expression of proteins involved in the Nrf2 oxidative stress response and autophagy (Fig. 6B-C, and Supplementary Fig. 8), and a lower increase in the expression of proteins involved in inflammatory and immune responses (Supplementary Fig. 9), compared to mice. The altered expression of representative proteins from these processes (NQO1, HMOX1, SQSTM1 and LC3B (*Map1lc3b*)) was confirmed at each time point in the two species via immunoblotting (Fig. 6D-I). Notably, in the case of LC3B, which is commonly used as a marker of autophagy (38), both the cytosolic LC3B-I and autophagosome-bound LC3B-II were expressed at higher levels in the livers of rats at the 0 h time point (Fig. 6H-I). In addition, whilst APAP induced autophagy at early time points in both species, as evidenced by both a decrease in abundance of SQSTM1 and the conversion of LC3B-I to LC3B-II at early time points, the level of LC3B-I was found to be consistently higher in the rat across the timeframe of the study (Fig. 6G-I), suggestive of a greater autophagic capacity. Together, these data support a more robust activation of adaptive

stress response pathways in rats compared with mice following exposure to an equivalent NAPQI insult.

Rats exhibit a higher basal hepatic expression of stress response pathway markers compared with mice and humans

Whilst our ‘omics analyses highlighted a clear difference between mice and rats in the inducible activity of several stress response pathways, the timeframe for altered expression of the associated proteins (> 6 h) relative to the rapid onset of liver injury (> 2 h) means that these adaptations could not have occurred swiftly enough to directly influence the different sensitivities of the species to the equivalent APAP insults. Given the limitations of probe-based microarray and qPCR data sets for comparing absolute gene expression levels across species, we used publicly available RNA-Seq (reads per kilobase million) data (31) to assess the basal expression levels of relevant genes in liver tissue from mice and rats, from birth to adulthood. This analysis highlighted the generally higher basal expression levels of a number of genes associated with the Nrf2 oxidative stress and endoplasmic reticulum stress responses and autophagic capacity in rats compared with mice (Fig. 7). These findings were supported by our proteomics data; grouping the normalised expression quantities of orthologous proteins from the 0 h control animals in the APAP study into bins confirmed the trend of higher basal expression of Nrf2 and autophagy-associated proteins in the livers of rats, compared with mice (Fig. 8). Notably, using the public RNA-Seq data, we also found that many genes from these processes were expressed at a higher basal level in the liver of rats than in humans, which overall better resembled mice (Fig. 7). We confirmed this at the protein level by immunoblot analysis of 0 h control tissues from animals in the APAP study, along with background liver tissue donated by eight

patients undergoing elective resection of hepatic tumours (Fig. 9A-B). Notably, the latter samples exhibited marked inter-individual variability in the expression levels of the analysed proteins (Fig. 9A-B). Taken together, these data indicate that rats exhibit a greater basal and adaptive capacity of hepatic stress responses than mice and humans.

DISCUSSION

Differences in metabolism and disposition are known to contribute to differences in species sensitivity to drug toxicity. However, less attention has been paid to the possibility that tissue stress response capacity may also contribute to cases of differential species susceptibility. We have used a combination of PBPK modelling and simulation coupled to multi-omics analysis to determine if differential sensitivity to APAP-induced liver injury in mice and rats is related to differences in metabolism or tissue response to equivalent burdens of the reactive intermediate NAPQI. Our study highlights the higher basal and inducible activity of the Nrf2 antioxidant and autophagy stress responses in the livers of rats, compared with mice and humans. Consistent with our findings, Xu et al. (39) reported that mice better resemble humans in terms of the basal hepatic expression of oxidative stress-related genes, whilst rats better resemble humans in terms of the expression of genes associated with lipid metabolism. Transgenic Nrf2 null mice have been reported to exhibit greater susceptibility to a large number of liver toxins, including APAP (40), whilst autophagy has been implicated in the pathogenesis of DILI (41) and shown to act as a defence mechanism in APAP hepatotoxicity by removing damaged mitochondria (42). The Nrf2 pathway and autophagy are linked by the p62/SQSTM1 (sequestosome 1) protein, which acts as a cargo receptor for autophagic degradation of ubiquitinated targets and activates Nrf2 by interfering with its ability to bind to its inhibitor Keap1 (20). SQSTM1 expression is also transcriptionally regulated by Nrf2, suggesting that SQSTM1 forms part of a regulatory feedback loop in the Nrf2 pathway (43). Notably, APAP protein adducts have been shown to be cleared at a faster rate in the livers of rats (44) compared with mice (45). Taken together, the differential activity of these and other

cytoprotective pathways is expected to influence species sensitivity to a range of chemical insults.

Rats are well known to be relatively resistant to APAP liver toxicity, compared with mice and other sensitive species (6), due in part to differences in the extent of drug bioactivation and detoxication. Indeed, Gregus et al. (12) previously demonstrated that mice excrete over 50 % of a dose of APAP as toxic bioactivation products (APAP-GSH and associated hydrolysis products) whereas rats excrete only 9 % of APAP via these routes. As a result of this and the greater excretion of detoxication pathway metabolites (APAP-glucuronide and -sulfate) in rats, the ratio of toxic bioactivation products versus detoxication pathway metabolites was found to be 10-fold higher in mice than rats (12). Consistent with these findings, Boobis et al. (14) reported that primary hepatocytes from mice and rats exhibit large differences in the extent of covalent binding and degree of toxicity following exposure to APAP in vitro. Notably, Tee et al. (13) provided evidence that rat hepatocytes are relatively resistant to depletion of GSH and covalent protein binding upon direct exposure to NAPQI in vitro, compared with hepatocytes from hamsters, which are known to be highly sensitive to APAP liver toxicity. To overcome these differences in metabolic fate of the drug and enable a fairer assessment of the tissue response of mice and rats to a comparable APAP insult, we used PBPK modelling and simulation to support the use of 300 and 1000 mg/kg APAP as OEDs yielding an equivalent total hepatic burden of NAPQI in mice and rats, respectively. Our results show that PBPK modelling and simulation successfully predicted OEDs resulting in comparable NAPQI burden between the mouse and rat. Despite this, rats remained more resistant to APAP hepatotoxicity compared with mice.

McGill et al. (6) also used 300 and 1000 mg/kg doses (albeit via intraperitoneal, rather than oral, administration) in their investigation of the biochemical events underlying the differential sensitivity of mice and rats, respectively, to APAP liver toxicity. Consistent with our findings, the authors reported a substantial increase in serum ALT activity and marked centrilobular necrosis in mice, with minimal responses observed in rats (6). Total APAP-protein adducts reached similar levels in the two species, confirming the equivalent degrees of chemical insult with these doses, and leading the authors to conclude that there are downstream factors responsible for the difference in sensitivity of mice and rats to APAP toxicity (6). In mice, JNK has been shown to undergo early phosphorylation and translocation to mitochondria partly as a result of the initial oxidative stress provoked by APAP (46, 47). Here, we have shown that p-JNK accumulates in liver samples from both mice and rats, peaking 3 h after APAP administration. In their study, McGill et al. (6) demonstrated that APAP-protein adducts and p-JNK translocation were consistently higher in mitochondrial fractions from mouse liver, and that rats therefore do not develop the critical levels of mitochondrial dysfunction or oxidative stress associated with APAP toxicity in mice. In light of our findings, it is possible that this is due to the greater capacity of the rat liver to cope with the initial chemical insult and mitigate against the progression of downstream toxic events.

Consistent with our finding of differences in the basal expression of stress response pathway components across liver tissues donated by eight patients, Kang et al. (48) recently reported quantitative differences in the drug-induced response of an Nrf2-associated gene set amongst primary hepatocytes isolated from different human donors. In addition, Liu et al. (49) have provided evidence that the hepatic expression

of Nrf2-regulated genes is altered in patients with certain liver diseases. Hence, whilst the stress response capacity of most humans likely sits within an average range, it is possible that some individuals have relatively higher or lower abilities to respond to chemical insults, which could influence inter-individual sensitivity to some drug toxicities.

A limitation of our in vivo study is that we have focused on only APAP as an exemplar hepatotoxic compound, and the C57Bl6/J and Sprague-Dawley strains of mouse and rat, respectively. Harrill et al. (50) have reported marked differences in sensitivity to the toxic effects of 300 mg/kg APAP across a panel of 36 inbred mouse strains, although C57Bl6/J mice were found to sit in the middle of this range, and the mechanism of APAP toxicity has been extensively investigated in this strain (6). In addition, our comparison of the basal expression of stress response pathway components used public transcriptomics data from CD-1 mice, alongside Sprague-Dawley rats (31). A retrospective evaluation of the preclinical toxicity studies conducted across 77 drug candidates by one large pharmaceutical company found that liver effects considered to be adaptive (e.g. hepatocellular hypertrophy, which is known to be associated with the Nrf2 and other stress responses (24)) were more than twice as prevalent in rats (39 % of cases; predominantly Han Wistar strain) than in non-rodents (16 % of cases) (51). In addition, Monroe et al. (52) recently demonstrated that a large number of drugs that form chemically reactive metabolites, and were terminated due to clinical liver toxicity, provoke an activation of hepatic Nrf2 signalling, despite a lack of overt liver injury, in the rat (mixture of Sprague-Dawley and Han Wistar strains). Hence, whilst there will likely be some differences between strains, these observations indicate that, in general, the rat liver is highly resistant to chemical

insult due to an increased capacity to respond to a range of stresses. Therefore, the rat may under-predict the sensitivity of other species, including humans, to certain drug toxicities such as those associated with the formation of reactive metabolites.

In the case of small molecule drugs, which make up a significant proportion of medicines submitted to global regulatory authorities each year, regulatory preclinical toxicity studies are expected to be performed in both a rodent and non-rodent species. The rat is by far the most commonly used rodent species, yet several studies have concluded that it is a relatively poor model for prediction of some human drug toxicities (1, 53). Our study has focussed on the liver, which is one of the most common targets of drug toxicity both preclinically and in patients (54). However, a broader understanding of the degree of conservation of stress responses and other key physiological traits in different organ systems across preclinical models and humans is vital to inform the selection of appropriate species for preclinical testing to best reflect the clinical setting. Such knowledge will also be useful for the parameterisation of computational tools that are being designed to support risk assessment as a new drug candidate transitions from the preclinical to the clinical sphere (55), therefore improving the efficiency of the drug development process and maximising patient safety.

REFERENCES

1. Olson H, Betton G, Robinson D, Thomas K, Monro A, Kolaja G, Lilly P, et al. Concordance of the toxicity of pharmaceuticals in humans and in animals. Regul Toxicol Pharmacol 2000;32:56-67.
2. Aithal GP. Mind the gap. Altern Lab Anim 2010;38 Suppl 1:1-4.
3. Smith MT. Mechanisms of troglitazone hepatotoxicity. Chem Res Toxicol 2003;16:679-687.
4. Leslie EM, Watkins PB, Kim RB, Brouwer KL. Differential inhibition of rat and human Na+-dependent taurocholate cotransporting polypeptide (NTCP/SLC10A1)by bosentan: a mechanism for species differences in hepatotoxicity. J Pharmacol Exp Ther 2007;321:1170-1178.
5. Lee WM, Larrey D, Olsson R, Lewis JH, Keisu M, Auclert L, Sheth S. Hepatic findings in long-term clinical trials of ximelagatran. Drug Saf 2005;28:351-370.
6. McGill MR, Williams CD, Xie Y, Ramachandran A, Jaeschke H. Acetaminophen-induced liver injury in rats and mice: comparison of protein adducts, mitochondrial dysfunction, and oxidative stress in the mechanism of toxicity. Toxicol Appl Pharmacol 2012;264:387-394.
7. Lee EW, Lai Y, Zhang H, Unadkat JD. Identification of the mitochondrial targeting signal of the human equilibrative nucleoside transporter 1 (hENT1): implications for interspecies differences in mitochondrial toxicity of fialuridine. J Biol Chem 2006;281:16700-16706.
8. Larson AM, Polson J, Fontana RJ, Davern TJ, Lalani E, Hynan LS, Reisch JS, et al. Acetaminophen-induced acute liver failure: results of a United States multicenter, prospective study. Hepatology 2005;42:1364-1372.
9. Bernal W, Auzinger G, Dhawan A, Wendon J. Acute liver failure. Lancet 2010;376:190-201.
10. Ramachandran A, Jaeschke H. Acetaminophen Hepatotoxicity. Semin Liver Dis 2019;39:221-234.
11. Yoon E, Babar A, Choudhary M, Kutner M, Pyrsopoulos N. Acetaminophen-Induced Hepatotoxicity: a Comprehensive Update. J Clin Transl Hepatol 2016;4:131-142.
12. Gregus Z, Madhu C, Klaassen CD. Species variation in toxication and detoxication of acetaminophen in vivo: a comparative study of biliary and urinary excretion of acetaminophen metabolites. J Pharmacol Exp Ther 1988;244:91-99.
13. Tee LB, Davies DS, Seddon CE, Boobis AR. Species differences in the hepatotoxicity of paracetamol are due to differences in the rate of conversion to its cytotoxic metabolite. Biochem Pharmacol 1987;36:1041-1052.
14. Boobis AR, Tee LB, Hampden CE, Davies DS. Freshly isolated hepatocytes as a model for studying the toxicity of paracetamol. Food Chem Toxicol 1986;24:731-736.
15. Jamei M, Dickinson GL, Rostami-Hodjegan A. A framework for assessing inter-individual variability in pharmacokinetics using virtual human populations and integrating general knowledge of physical chemistry, biology, anatomy, physiology and genetics: A tale of 'bottom-up' vs 'top-down' recognition of covariates. Drug Metab Pharmacokinet 2009;24:53-75.
16. Jamei M, Marciniak S, Edwards D, Wragg K, Feng K, Barnett A, Rostami-Hodjegan A. The simcyp population based simulator: architecture, implementation, and quality assurance. In Silico Pharmacol 2013;1:9.
17. Musther H, Harwood MD, Yang J, Turner DB, Rostami-Hodjegan A, Jamei M. The Constraints, Construction, and Verification of a Strain-Specific Physiologically Based Pharmacokinetic Rat Model. J Pharm Sci 2017;106:2826-2838.
18. Rowland Yeo K, Jamei M, Yang J, Tucker GT, Rostami-Hodjegan A. Physiologically based mechanistic modelling to predict complex drug-drug interactions involving simultaneous competitive and time-dependent enzyme inhibition by parent compound

and its metabolite in both liver and gut - the effect of diltiazem on the time-course of exposure to triazolam. Eur J Pharm Sci 2010;39:298-309.
19. Vandeputte C, Guizon I, Genestie-Denis I, Vannier B, Lorenzon G. A microtiter plate assay for total glutathione and glutathione disulfide contents in cultured/isolated cells: performance study of a new miniaturized protocol. Cell Biol Toxicol 1994;10:415-421.
20. Copple IM, Lister A, Obeng AD, Kitteringham NR, Jenkins RE, Layfield R, Foster BJ, et al. Physical and functional interaction of sequestosome 1 with Keap1 regulates the Keap1-Nrf2 cell defense pathway. J Biol Chem 2010;285:16782-16788.
21. Gautier L, Cope L, Bolstad BM, Irizarry RA. affy--analysis of Affymetrix GeneChip data at the probe level. Bioinformatics 2004;20:307-315.
22. Dai M, Wang P, Boyd AD, Kostov G, Athey B, Jones EG, Bunney WE, et al. Evolving gene/transcript definitions significantly alter the interpretation of GeneChip data. Nucleic Acids Res 2005;33:e175.
23. Ritchie ME, Phipson B, Wu D, Hu Y, Law CW, Shi W, Smyth GK. limma powers differential expression analyses for RNA-sequencing and microarray studies. Nucleic Acids Res 2015;43:e47.
24. Sutherland JJ, Webster YW, Willy JA, Searfoss GH, Goldstein KM, Irizarry AR, Hall DG, et al. Toxicogenomic module associations with pathogenesis: a network-based approach to understanding drug toxicity. Pharmacogenomics J 2018;18:377-390.
25. Yu G, Wang LG, Han Y, He QY. clusterProfiler: an R package for comparing biological themes among gene clusters. OMICS 2012;16:284-287.
26. Ashburner M, Ball CA, Blake JA, Botstein D, Butler H, Cherry JM, Davis AP, et al. Gene ontology: tool for the unification of biology. The Gene Ontology Consortium. Nat Genet 2000;25:25-29.
27. Andersen CL, Jensen JL, Orntoft TF. Normalization of real-time quantitative reverse transcription-PCR data: a model-based variance estimation approach to identify genes suited for normalization, applied to bladder and colon cancer data sets. Cancer Res 2004;64:5245-5250.
28. Demichev V, Messner CB, Vernardis SI, Lilley KS, Ralser M. DIA-NN: neural networks and interference correction enable deep proteome coverage in high throughput. Nat Methods 2020;17:41-44.
29. Zhu Y, Orre LM, Zhou Tran Y, Mermelekas G, Johansson HJ, Malyutina A, Anders S, et al. DEqMS: A Method for Accurate Variance Estimation in Differential Protein Expression Analysis. Mol Cell Proteomics 2020;19:1047-1057.
30. Wang S, García-Seisdedos D, Prakash A, Kundu DJ, Collins A, George N, Fexova S, et al. Integrated view and comparative analysis of baseline protein expression in mouse and rat tissues. bioRxiv 2021.
31. Cardoso-Moreira M, Halbert J, Valloton D, Velten B, Chen C, Shao Y, Liechti A, et al. Gene expression across mammalian organ development. Nature 2019;571:505-509.
32. Ito Y, Bethea NW, Abril ER, McCuskey RS. Early hepatic microvascular injury in response to acetaminophen toxicity. Microcirculation 2003;10:391-400.
33. Corcoran GB, Wong BK. Role of glutathione in prevention of acetaminophen-induced hepatotoxicity by N-acetyl-L-cysteine in vivo: studies with N-acetyl-D-cysteine in mice. J Pharmacol Exp Ther 1986;238:54-61.
34. Chun Y, Kim J. Autophagy: An Essential Degradation Program for Cellular Homeostasis and Life. Cells 2018;7.
35. Mesnage R, Defarge N, Rocque LM, Spiroux de Vendomois J, Seralini GE. Laboratory Rodent Diets Contain Toxic Levels of Environmental Contaminants: Implications for Regulatory Tests. PLoS One 2015;10:e0128429.
36. Lau A, Whitman SA, Jaramillo MC, Zhang DD. Arsenic-mediated activation of the Nrf2-Keap1 antioxidant pathway. J Biochem Mol Toxicol 2013;27:99-105.
37. Janasik B, Reszka E, Stanislawska M, Jablonska E, Kuras R, Wieczorek E, Malachowska B, et al. Effect of Arsenic Exposure on NRF2-KEAP1 Pathway and Epigenetic Modification. Biol Trace Elem Res 2018;185:11-19.

38. Mizushima N, Yoshimori T. How to interpret LC3 immunoblotting. Autophagy 2007;3:542-545.
39. Xu Z, Kang Q, Yu Z, Tian L, Zhang J, Wang T. Research on the Species Difference of the Hepatotoxicity of Medicine Based on Transcriptome. Front Pharmacol 2021;12:647084.
40. Clarke JL, Murray JB, Park BK, Copple IM. Roles of Nrf2 in drug and chemical toxicity. Current Opinion in Toxicology 2016;1:104-110.
41. Chen S, Melchior WB, Jr., Wu Y, Guo L. Autophagy in drug-induced liver toxicity. J Food Drug Anal 2014;22:161-168.
42. Ni HM, Bockus A, Boggess N, Jaeschke H, Ding WX. Activation of autophagy protects against acetaminophen-induced hepatotoxicity. Hepatology 2012;55:222-232.
43. Jiang T, Harder B, Rojo de la Vega M, Wong PK, Chapman E, Zhang DD. p62 links autophagy and Nrf2 signaling. Free Radic Biol Med 2015;88:199-204.
44. Tarloff JB, Khairallah EA, Cohen SD, Goldstein RS. Sex- and age-dependent acetaminophen hepato- and nephrotoxicity in Sprague-Dawley rats: role of tissue accumulation, nonprotein sulfhydryl depletion, and covalent binding. Fundam Appl Toxicol 1996;30:13-22.
45. Henderson CJ, Wolf CR, Kitteringham N, Powell H, Otto D, Park BK. Increased resistance to acetaminophen hepatotoxicity in mice lacking glutathione S-transferase Pi. Proc Natl Acad Sci U S A 2000;97:12741-12745.
46. Gunawan BK, Liu ZX, Han D, Hanawa N, Gaarde WA, Kaplowitz N. c-Jun N-terminal kinase plays a major role in murine acetaminophen hepatotoxicity. Gastroenterology 2006;131:165-178.
47. Saito C, Lemasters JJ, Jaeschke H. c-Jun N-terminal kinase modulates oxidant stress and peroxynitrite formation independent of inducible nitric oxide synthase in acetaminophen hepatotoxicity. Toxicol Appl Pharmacol 2010;246:8-17.
48. Kang W, Podtelezhnikov AA, Tanis KQ, Pacchione S, Su M, Bleicher KB, Wang Z, et al. Development and Application of a Transcriptomic Signature of Bioactivation in an Advanced In Vitro Liver Model to Reduce Drug-induced Liver Injury Risk Early in the Pharmaceutical Pipeline. Toxicol Sci 2020;177:121-139.
49. Liu J, Cui JY, Lu YF, Corton JC, Klaassen CD. Sex-, Age-, and Race/Ethnicity-Dependent Variations in Drug-Processing and NRF2-Regulated Genes in Human Livers. Drug Metab Dispos 2021;49:111-119.
50. Harrill AH, Watkins PB, Su S, Ross PK, Harbourt DE, Stylianou IM, Boorman GA, et al. Mouse population-guided resequencing reveals that variants in CD44 contribute to acetaminophen-induced liver injury in humans. Genome Res 2009;19:1507-1515.
51. Horner S, Ryan D, Robinson S, Callander R, Stamp K, Roberts RA. Target organ toxicities in studies conducted to support first time in man dosing: an analysis across species and therapy areas. Regul Toxicol Pharmacol 2013;65:334-343.
52. Monroe JJ, Tanis KQ, Podtelezhnikov AA, Nguyen T, Machotka SV, Lynch D, Evers R, et al. Application of a Rat Liver Drug Bioactivation Transcriptional Response Assay Early in Drug Development That Informs Chemically Reactive Metabolite Formation and Potential for Drug-induced Liver Injury. Toxicol Sci 2020;177:281-299.
53. Greaves P, Williams A, Eve M. First dose of potential new medicines to humans: how animals help. Nat Rev Drug Discov 2004;3:226-236.
54. Wilke RA, Lin DW, Roden DM, Watkins PB, Flockhart D, Zineh I, Giacomini KM, et al. Identifying genetic risk factors for serious adverse drug reactions: current progress and challenges. Nat Rev Drug Discov 2007;6:904-916.
55. Weaver RJ, Blomme EA, Chadwick AE, Copple IM, Gerets HHJ, Goldring CE, Guillouzo A, et al. Managing the challenge of drug-induced liver injury: a roadmap for the development and deployment of preclinical predictive models. Nat Rev Drug Discov 2020;19:131-148.

FIGURES

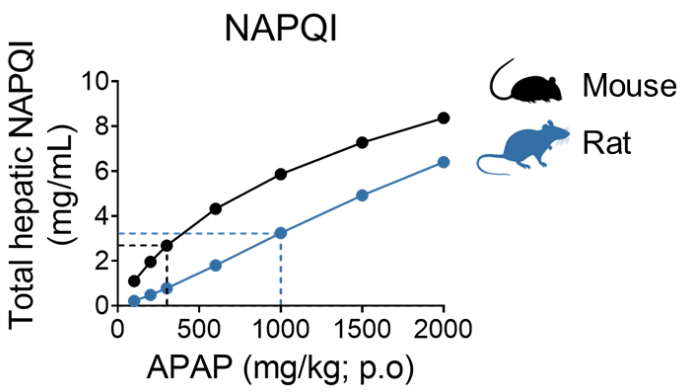

Figure 1. Identification of pharmacokinetically equivalent doses of APAP in mice and rats.

Oral equivalent doses (OEDs) of APAP derived from PBPK model simulations that were predicted to give similar levels of total hepatic NAPQI burden in mice (300 mg/kg) and rats (1000 mg/kg).

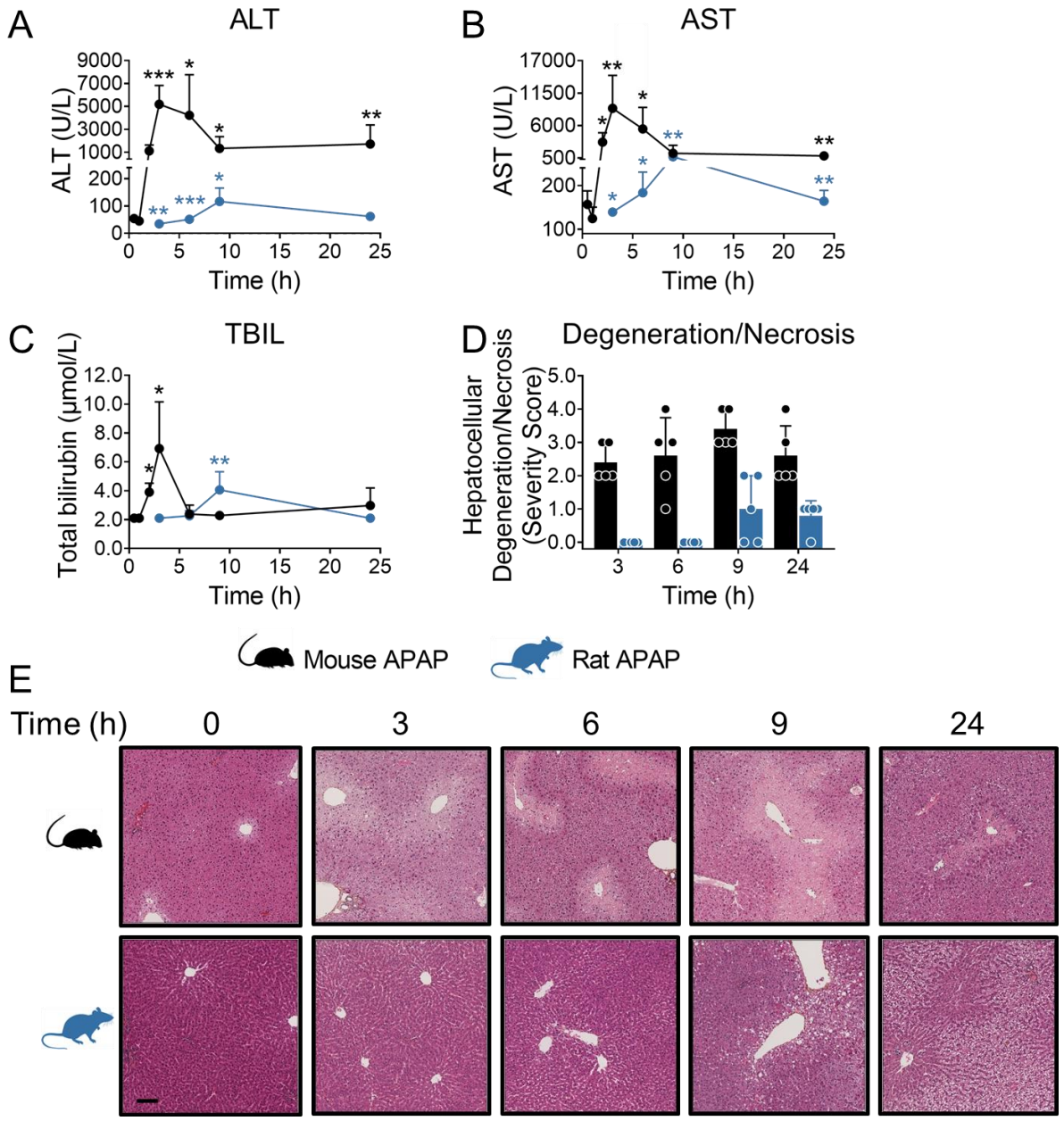

Figure 2. Hepatocellular injury after equivalent hepatic NAPQI burden occurs more quickly and to a greater magnitude in mice compared to rats.

Liver injury serum markers (ALT (**A**), AST (**B**) and total bilirubin (TBIL, **C**)) and hepatocellular degeneration/necrosis (**D**) in C57BL/6J mice (0.5, 1, 2, 3, 6, 9 and 24 h) and Sprague-Dawley rats (3, 6, 9 and 24 h) exposed to 300 mg/kg and 1000 mg/kg APAP, respectively. Time-matched vehicle control groups were given 1 % (w/v) hydroxyethylcellulose. The extent of centrilobular hepatocellular degeneration/

necrosis was assigned a semi-quantitative score as follows: 0 = none observed, 1 = minimal, 2 = mild, 3 = moderate, 4 = marked and 5 = severe. Values are mean ± SD (n=5). In (**D**) severity scores are shown for each animal. Statistical significance was determined against time-matched vehicle control (Supplementary Figure 2). P-values are denoted as *p<0.05, **p<0.01, or ***p<0.001. (**E**) Representative images of hematoxylin-eosin saffron stained liver sections from mice and rats at baseline (0 h) or treated with APAP at the indicated time points. Scale bar = 100 μm.

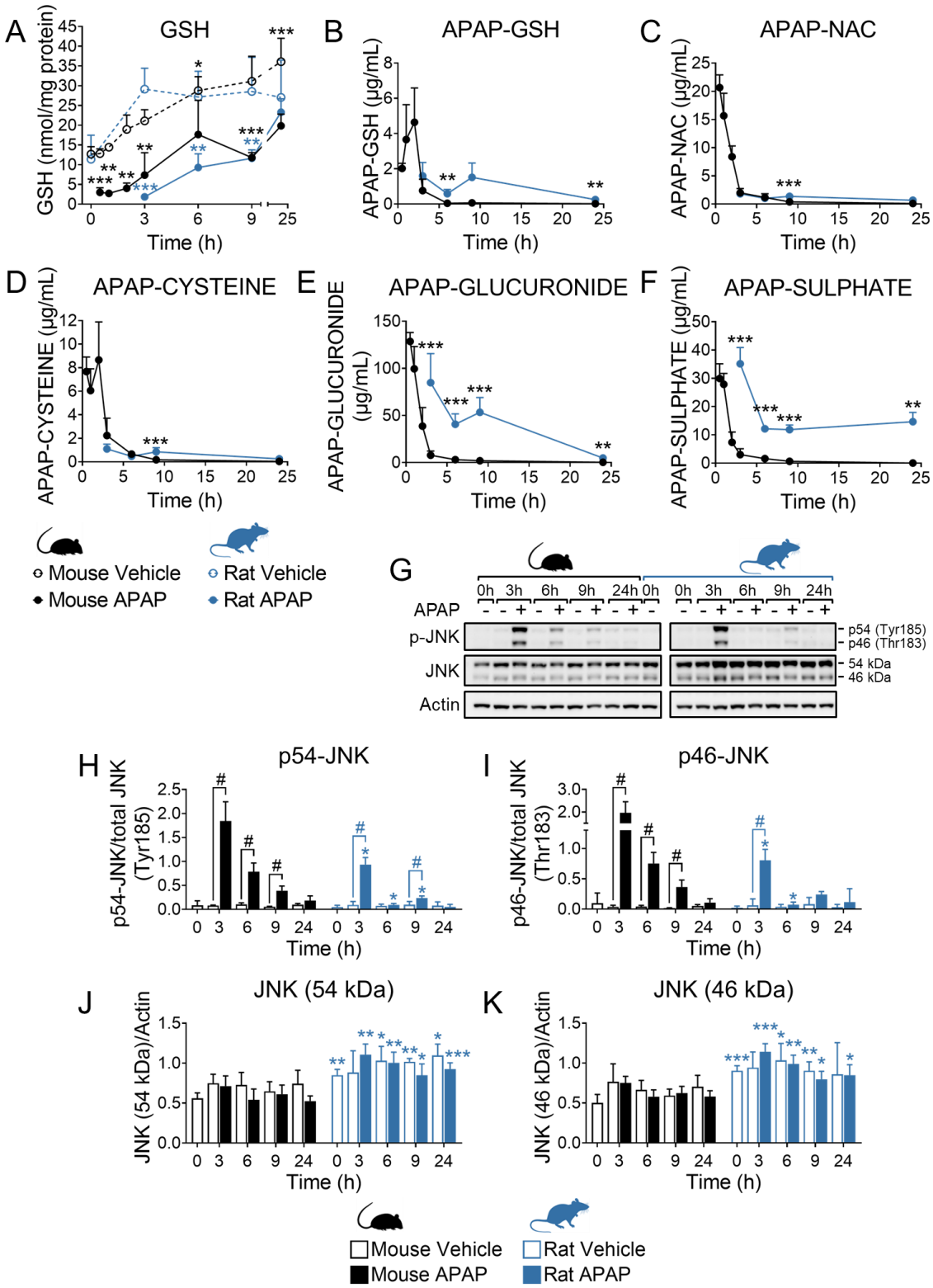

Figure 3. Confirmation of equivalent chemical insult in mice and rats.

Total hepatic GSH (**A**) and APAP metabolites (APAP-GSH (**B**), APAP-NAC (**C**), APAP-Cysteine (**D**), APAP-Glucuronide (**E**) and APAP-Sulphate (**F**)) in the plasma of

C57BL/6J mice (0.5, 1, 2, 3, 6, 9 and 24 h) and Sprague-Dawley rats (3, 6, 9 and 24 h) exposed to 300 mg/kg and 1000 mg/kg APAP respectively were quantified. Values are mean ± SD (n=5-12 in A, n=5 in B-F). Statistical significance of total hepatic GSH was determined per species against time-matched control (dotted lines) whilst for each APAP metabolite, statistical significance was determined between APAP-treated mice and rats where possible per time point. Unpaired t-test or Mann-Whitney U test, as appropriate. P-values are denoted as *p<0.05, **p<0.01, ***p<0.001, or ****p<0.0001. (**G**) APAP-induced phosphorylation of c-Jun N-terminal kinase (JNK) at Tyr185 (p56) and Thr183 (p46). Samples are pooled from 5 animals per time point. (**H-J**) Densitometric analysis of immunoblots. Protein levels were normalised to total JNK (**H-I**) or β-actin (**J-K**)**.** Values are mean ± SD (n=4). Unpaired t-test or Mann-Whitney U test, as appropriate. P-values are denoted as *p<0.05, **p<0.01, or ***p<0.001, comparison mouse versus rat for each condition/time point, or $^{\#}$p<0.05, comparison APAP-treated animals versus vehicle controls, as indicated.

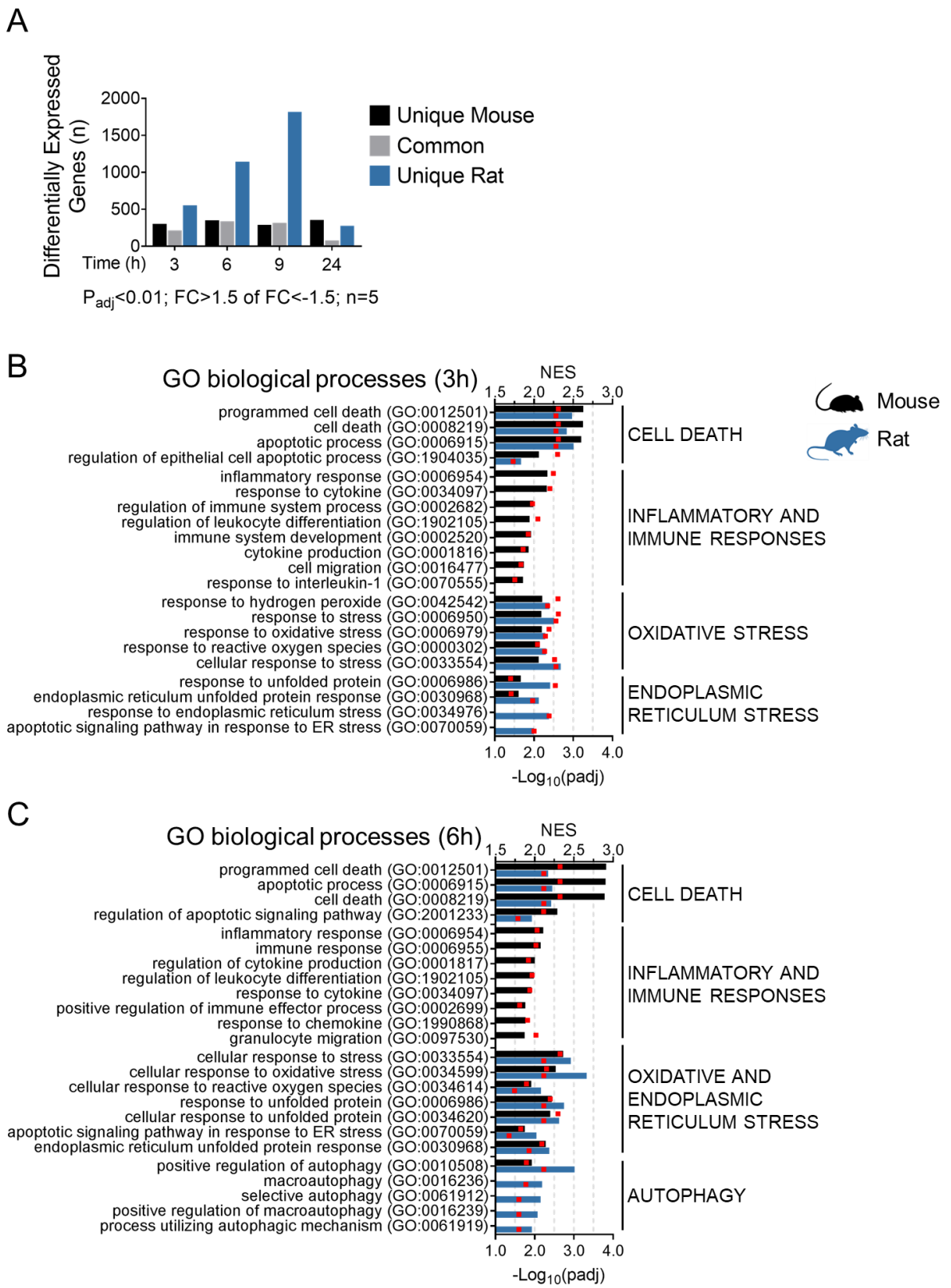

Figure 4. Transcriptomic analysis reveals a more robust activation of adaptive stress response pathways in the liver of APAP-treated rats, compared with mice.

(**A**) Number of Differentially Expressed Genes (DEGs; Padj < 0.01, fold change >1.5 or <-1.5; comparison against time matched vehicle controls). Black and blue bars represent the number of genes that were uniquely responsive to APAP in mice and rat, respectively. Stacked grey bars indicate DEGs in common between the two species. Gene Set Enrichment Analysis (GSEA) at (**B**) 3 and (**C**) 6 hours after APAP treatment. Bars represent normalised enrichment scores (NES) of selected gene onotology (GO) terms for both species (mouse in black, rat in blue). Individual GO terms ($P_{adj} < 0.05$) were clustered into parent terms. The bar is missing for non-significant GO terms. Red squares represent $-\log_{10}$ of P_{adj}. See Supplementary File S1 for the full analysis at all time points.

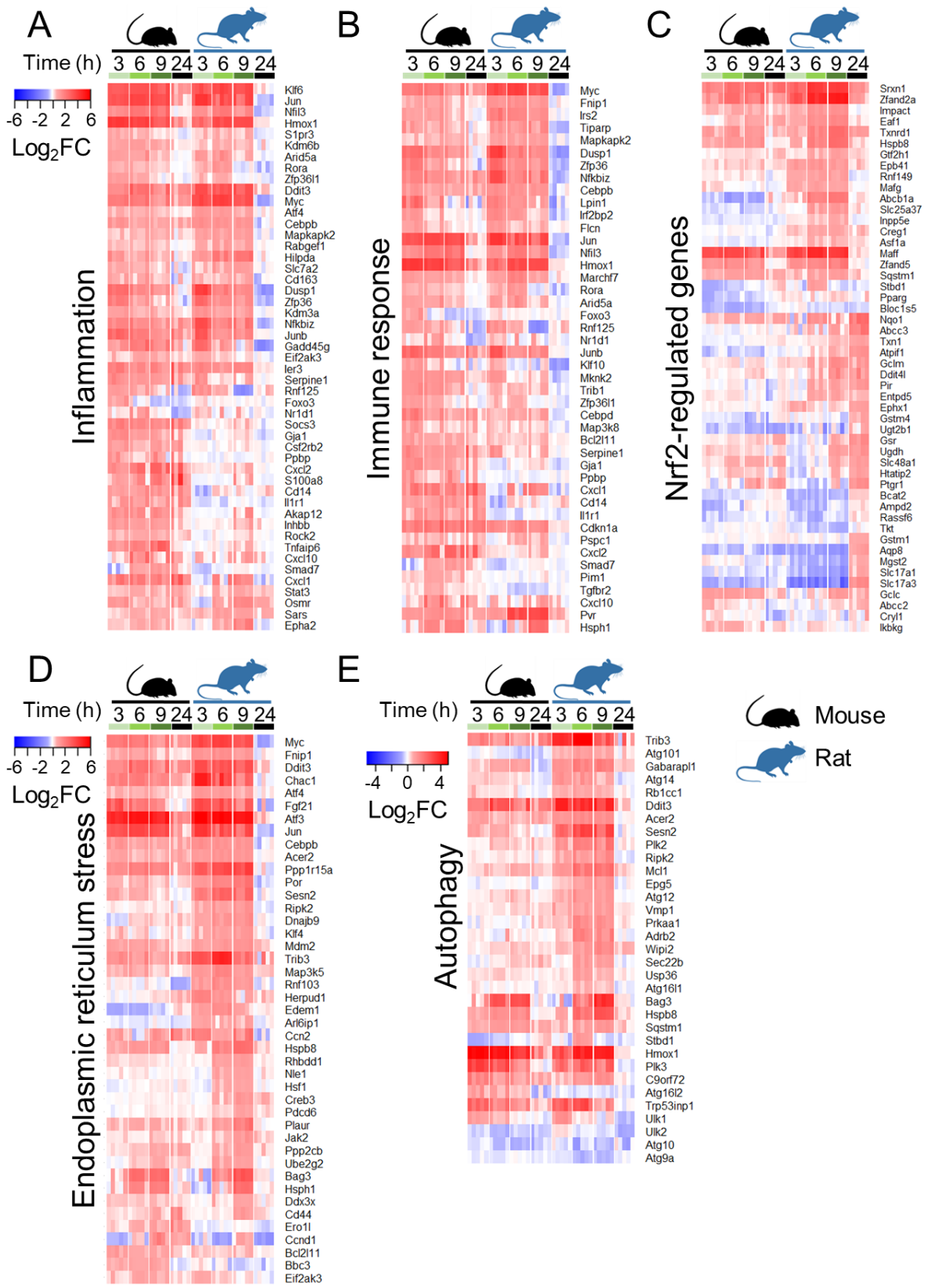

Figure 5. Gene level confirmation of the more robust activation of adaptive stress responses in the rat liver.

Heatmaps showing changes in the expression of genes regulating (**A**) inflammatory, (**B**) immune, (**C**) oxidative stress, (**D**) endoplasmic reticulum (ER) stress responses, and (**E**) autophagy in the liver of C57BL/6J mice and Sprague Dawley rats treated with 300 mg/kg and 1000 mg/kg APAP, respectively (n=5/group) at 3, 6, 9, and 24 hours. Data are expressed as $\log_2$ fold-change *versus* time-matched vehicle control animals.

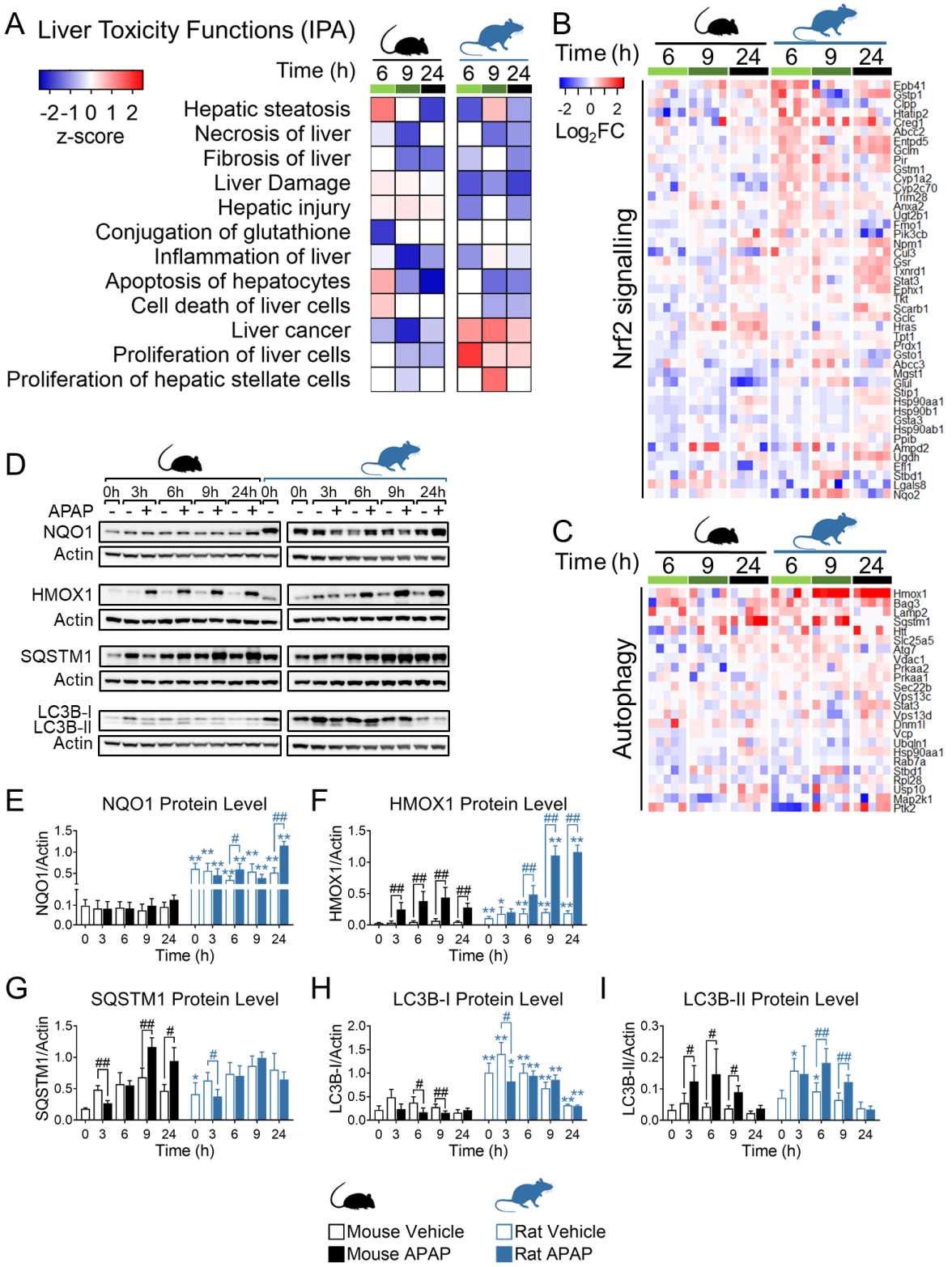

Figure 6. Proteomic analysis corroborates the more robust activation of adaptive stress response pathways in the liver of APAP-treated rats, compared with mice.

(**A**) Comparative toxicity analysis (IPA-Tox) in the liver of mice and rats treated with 300 mg/kg and 1000 mg/kg APAP, respectively (n=5/group) at 6, 9, and 24 hours (SWATH proteomics). For each function a z-score was calculated at each time point against time-matched vehicle control animals. Heatmap plots showing changes in the expression of proteins involved in (**B**) Nrf2-signalling, and (**C**) autophagy. In (**B**) and (**C**), data are expressed as $\log_2$ fold-change *versus* time-matched vehicle control animals. (**D**) Protein expression levels of NAD(P)H dehydrogenase quinone 1 (NQO1), heme oxygenase 1(HMOX1), sequestosome 1 (SQSTM1), autophagy marker light chain 3 isoform B-I (LC3B-I) and -II (LC3B-II) at the indicated times after APAP or vehicle. Samples are pooled from 5 animals per time point. (**E-I**) Densitometric analysis of immunoblots. Protein levels were normalised to β-actin. Samples are pooled from 5 animals per time point. Values are mean ± SD (n=5). Mann-Whitney U test. P-values are denoted as $^{*}p<0.05$, and $^{**}p<0.01$, comparison mouse versus rat for each condition/time point, or $^{\#}p<0.05$, and $^{\#\#}p<0.01$, comparison APAP-treated animals *versus* vehicle controls, as indicated.

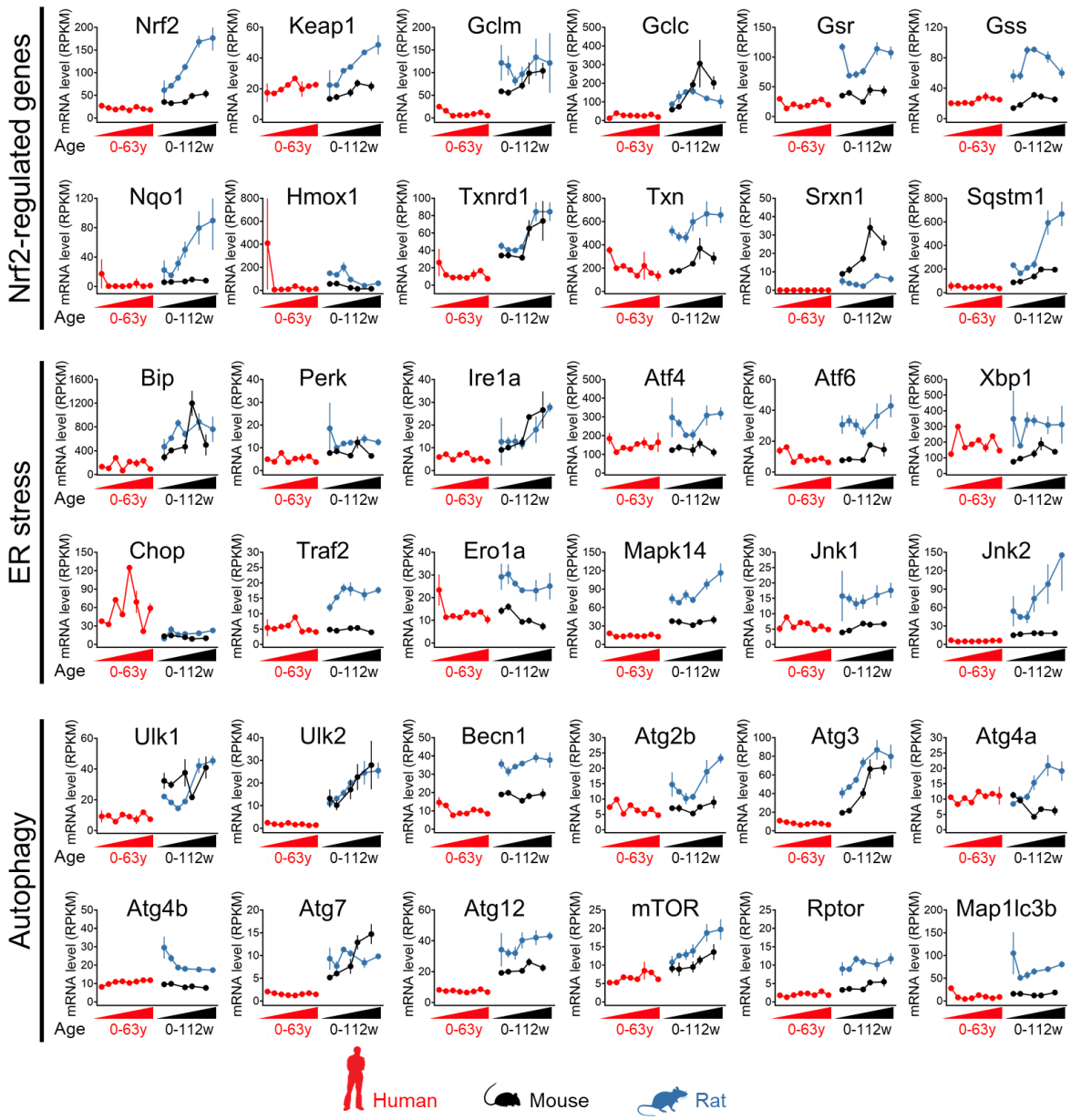

Figure 7. Higher basal expression levels of stress response pathway genes in the liver of rats, compared with mice and humans.

Differences between species in the basal expression of Nrf2 genes and genes modulating endoplasmic reticulum (ER) stress and autophagy from birth to adulthood. mRNA levels are express as reads per kilo base per million (RPKM) ± SD (31). Human samples were grouped as follows : “neonates”, “infants” (6-9 months), “toddlers” (2-4 years), “school” (7-9 years), “teenagers” (13-19 years), “adults” (25-32 years), “middle-

aged” (45-54 years), and “seniors” (58-63 years). Mouse samples (CD-1) were collected at week 0, 3, 14, 28, and 63, whereas rat samples (Sprague-Dawley) were collected at week 0, 3, 7, 14, 42, and 112.

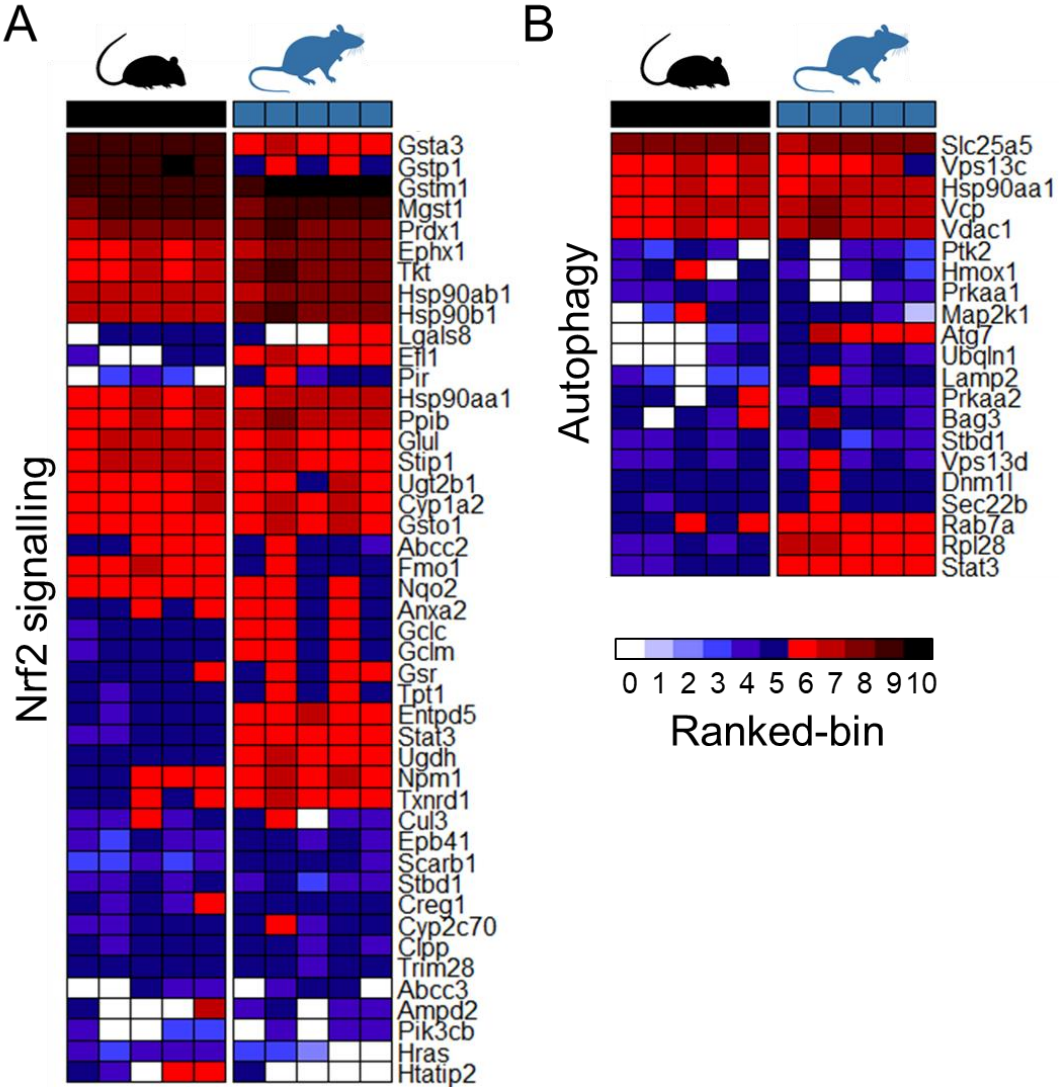

Figure 8. Higher basal expression levels of stress response pathway proteins in the liver of rats, compared with mice.

Heatmaps showing basal expression levels of proteins associated with the (**A**) Nrf2 and (**B**) autophagy responses in the liver of untreated C57BL/6J mice and Sprague-Dawley rats (0 h controls, n=5/species). Log_2 transformed normalised protein expression values from SWATH proteomics were ranked and grouped into 10 bins, wherein proteins with the lowest abundance were assigned to bin 1, and those with the highest abundance to bin 10. A bin value of 0 (depicted in white) was assigned to

proteins that were not detected. The difference amongst consecutive bins is 1.49 ± 0.16 ($\log_2$ expression).

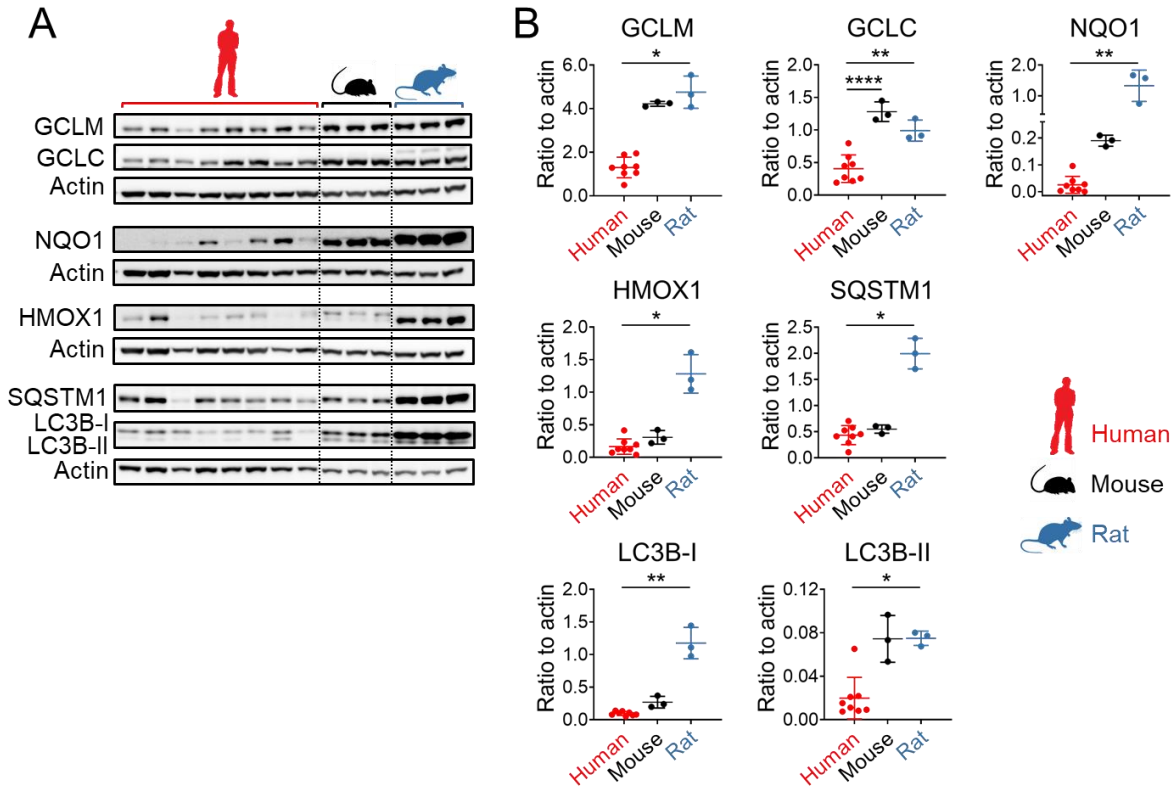

Figure 9. Confirmation of species differences in basal capacities of the Nrf2 and autophagy pathways.

Differences in basal antioxidant activity and autophagic capacity across species. (**A**) Densitometric analysis and (**B**) protein expression levels of GCLM, GCLC, NQO1, HMOX1, SQSTM1, and LC3B in liver tissue collected from patients undergoing liver resections (n=8) or untreated C57BL/6J mice (n=3) and Sprague-Dawley rats (n=3). Protein levels were normalised to β-actin. Values are mean ± SD (n=3). One-way ANOVA or Kruskal-Wallis test, as appropriate. P-values are denoted as *p<0.05, **p<0.01, and ****p<0.0001, comparison as indicated.